Available online at www.sciencedirect.com
SCIENCE DIRECT®
Journal of Computational Physics 201 (2004) 204–223
JOURNAL OF COMPUTATIONAL PHYSICS
www.elsevier.com/locate/jcp

Preconditioned spectral multi-domain discretization of the incompressible Navier–Stokes equations

Marcello Manna [a,*], Andrea Vacca [b], Michel O. Deville [c]

[a] *Dipartimento di Ingegneria Meccanica per l'Energetica, Università di Napoli "Federico II", Via Claudio 21, 80125 Naples, Italy*
[b] *Dipartimento di Ingegneria Civile, Seconda Università di Napoli, Via Roma 29, 81031 Aversa (Ce), Italy*
[c] *Laboratoire d'ingénierie numérique, École Polytechnique Fédérale de Lausanne, CH-1015 Lausanne, Switzerland*

Received 30 September 2003; received in revised form 18 May 2004; accepted 18 May 2004
Available online 17 June 2004

Abstract

In this paper we present a preconditioned multi-domain algorithm applied to the elliptic kernels arising from the spectral collocation of the incompressible Navier–Stokes equations in three space dimensions with one homogeneous direction. The technique, based on the iterative solution of the Schur complement matrix, allows for efficient numerical solution of the operators in complex geometries consisting of a collection of non-overlapping rectangular subdomains. The method is shown to be nearly optimal in terms of condition number behavior in a double path of refinement strategy, i.e. whenever both the number of Legendre modes and the number of subdomains are significantly increased. It is thus well suited for engineering applications in the fields of direct numerical simulation and large eddy simulation of turbulence.

1. Introduction

Direct numerical simulations (DNSs) of turbulent flows have been mainly carried out in the low Reynolds number range [1–4], and, as today, and despite the tremendous push in the development of new hardware, the extension to higher and more realistic flow regimes appears troublesome [5]. There is a general consensus, instead, that large eddy simulations (LESs) will allow for a significant increase of the Reynolds number range, and thus bear the promise of a considerable turbulence know-how improvement. This explains the huge efforts devoted to the development of more and more sophisticated (and expensive) subgrid scale models [6,7]; unfortunately none of the available models is capable of correctly describing in a statistical sense the near wall features, and most noticeably the existence of the relevant coherent structures responsible for turbulence production [8]. If the anisotropic near wall scales cannot be properly modeled the

* Corresponding author. Tel.: +39-81-768-3287; fax: +39-81-239-4165.
E-mail address: manna@unina.it (M. Manna).

0021-9991/$ - see front matter © 2004 Elsevier Inc. All rights reserved.
doi:10.1016/j.jcp.2004.05.011

only remaining alternative is to resolve them, a fact that requires appropriate numerical tools. Higher order methods (spectral or h–p type finite element methods) offer significant advantages over low order finite difference or finite volume methods both in terms of computational efficiency and numerical errors control. Multi-domain spectral methods combine the geometric flexibility of h–p type finite element methods with the exponential error decay typical of spectral discretization [9,10]. The spectral element method (SEM) of Patera [11] and Maday and Patera [12] is one such example which heavily relies on variational projection operators and Gauss numerical quadrature to generate the discrete equations. This set of equations constitute a large global system which requires efficient iterative preconditioned procedures [13]. The spectral element method offers efficient preconditioned solvers that were applied to CFD problems, e.g. for example the papers by Fischer and Tufo [14,15] on large scale parallel applications and the domain decomposition solvers proposed by Rønquist [16,17].

Non-variational multi-domain spectral methods based on explicit patching techniques are also available [18]. In the non-variational approach a C^1 continuity condition across the elemental boundaries is strongly enforced, and distinction is made between interior and interface unknowns. In between the two families of methods is the projection decomposition method (PDM) of Gervasio et al. [19], where, in a variational context (like in [11]), the original problem is decoupled into boundary value problems (one in each subdomain) and a problem on the interfaces between subdomains. In the PDM the equation expressing the continuity of the co-normal derivatives across the interface between the subdomains (Steklov–Poincaré interface) is solved by a Galerkin method using well conditioned basis. In [19] it has been shown that the above formulation is computationally highly efficient and leads to a linear system with condition number independent on the degree of the spectral approximation and mildly dependent on the number of subdomains. Applications of the PDM to the Navier–Stokes equations can be found in [20]. The non-conforming discretization of [13], which is essentially based upon the mortar element method (MEM) of Bernardi et al. [21], is closer to the PDM than to the SEM of Patera. The main difference is that the continuity condition on the interfaces is equivalent to collocation enforcement in the conformal SEM and obeys an integral matching relation in the MEM (viz. the solution does not belong to $\mathbb{H}^1(\Omega)$). It has been shown that the pointwise matching condition of SEM is not optimal when enforced in the MEM approach [21].

The present multi-domain method (MDM) is not a discontinuous Galerkin (dG) method because it is not set up in a flux formulation. However, the present methodology has some connections with the dG approach and the reader who is interested in this topic should consult the paper by Arnold et al. [22] that presents a unified framework to describe the various types of discontinuous methods. The multi-domain spectral method enforces a weak C^1 continuity between the sub-domains while dG allows the jumps in numerical fluxes. The imposition of consistency, boundedness and stability of the dG approximations makes them close albeit different from MDM.

The spectral multi-domain algorithm presented herein shares similarities with [19] in the following sense: the original elliptic problem is split into two separate problems, one for the interface unknowns and the other for the inner values. However, unlike [19] where the equivalent Schur complement matrix is designed to be well conditioned in some sense, we construct algebraic (one and two levels) preconditioners for the discrete counterpart of the Steklov–Poincaré operator (Schur matrix) exhibiting nearly optimal behaviors of the underlying iterative solver.

In simple geometries one level preconditioners of the Schur complement matrix are shown to be reasonably effective, in agreement with the findings of Couzy and Deville [23]. Conversely, in complex environments, the two level class of preconditioners [24], largely used in the finite element or finite difference framework, are found truly superior with respect to all challengers. The algorithms presented in this work share similarities with the optimal iterative substructuring methods of Pavarino and Widlund [25], and Casarin [26], along with the overlapping Schwarz techniques of Pavarino and Warburton [27], and prove comparable both in terms of performance and computational costs for shape regular subdomains (nearly isotropic grids). Here distinction has to be made between optimality and scalability; while the former refers

to the boundness of the condition number with the polynomials degree of the underlying approximation, the latter refers to the independence upon the number of subdomains.

The method is shown to be quasi-optimal and scalable in the isotropic case (in good agreement with the theoretical and numerical estimates reported in [25,26]). In the anisotropic case we are not aware of any quantitative results, although this is a frequently encountered scenario in wall bounded turbulent flows; our data indicate that present algorithms are optimal and quasi-scalable. Thus the methods are shown to be fully competitive with the PDM in the isotropic model problems, and to overwhelm it in presence of strong anisotropies.

Evidences of the above claims are provided comparing the performances of the methods on large scale model problems, viz. the Helmholtz and Poisson equations arising from the discretization of the semi-implicit incompressible Navier–Stokes equations in a time splitting formulation.

Direct and large eddy simulations of turbulent channel flow are carried out to validate the proposed methodology on highly anisotropic subdomains partitions.

The outline of the paper is as follows. In Section 2 we present the temporal and spatial discretization of the governing equations. In Section 3 the weak Legendre algorithm for the elliptic equations in a multi-domain framework is discussed. Issues concerning the numerical solution of the elliptic kernel and several algebraic preconditioners are presented in Section 4. Results both for model problems and full Navier–Stokes equations are provided in Section 5. Conclusions are given in Section 6.

2. Governing equations

In this work we are primarily interested in the discretization of the unsteady, incompressible Navier–Stokes equations in a complex domain $\tilde{\Omega} \subset \mathbb{R}^3$, with smooth boundaries $\partial\tilde{\Omega}$

$$\begin{aligned} &\frac{\partial u_i}{\partial t} + u_j \frac{\partial u_i}{\partial x_j} = -\frac{\partial p}{\partial x_i} + \frac{1}{Re}\frac{\partial^2 u_i}{\partial x_j^2} + f_i \quad \text{in } \tilde{\Omega}, \\ &\frac{\partial u_j}{\partial x_j} = 0 \quad \text{in } \tilde{\Omega}, \end{aligned} \tag{1}$$

where $(x_1, x_2, x_3) = (x, y, z)$ and t are the space and time coordinates, u_i are the non-dimensional velocity components, p is the non-dimensional pressure, and f_i are external force components. The Reynolds number $Re = v\ell/\nu$ is based on the kinematic viscosity ν and appropriate velocity and length scales (v and ℓ). Eqs. (1) are subject to a suitable set of initial and boundary conditions:

$$\begin{aligned} &u_i(\cdot, 0) = u_i^0(\cdot) \qquad \text{in } \tilde{\Omega}, \\ &u_i(\cdot, t) = \tilde{u}_i(\cdot) \qquad \text{on } \partial\tilde{\Omega}, \end{aligned} \tag{2}$$

with $u_i^0(\cdot)$ divergence free.

We next discuss the time discretization of (1), which is carried out with the second order projection scheme of Van Kan [28]. With the simulation of wall bounded turbulent flows in mind, for which the resolution requirements are necessarily very strict, we have chosen to treat the viscous terms implicitly to overcome the severe restriction of the time step that arises from the grid spacing in the wall normal direction. Thus the linear parabolic operator is approximated with a Crank–Nicolson scheme, while the non-linear terms are treated explicitly with a second order Adams–Bashforth scheme. Let u_i^n be the approximation to $u_i(\cdot, n\Delta t)$ at time level $n\Delta t$, and v_i the intermediate velocity vector field of the time splitting method whose curl approximates the curl of u_i, up to $\mathcal{O}(\Delta t)^2$. With these assumptions, and denoting with $\mathcal{N}_i$ the non-linear convective terms, the semi-discrete form of (1) reads

$$\frac{v_i - u_i^n}{\Delta t} - \frac{1}{2Re}\frac{\partial^2(v_i + u_i^n)}{\partial x_j^2} = -\frac{\partial p^n}{\partial x_i} - \frac{3}{2}\mathcal{N}_i^n + \frac{1}{2}\mathcal{N}_i^{n-1}, \tag{3}$$

$$\frac{u_i^{n+1} - v_i}{\Delta t} = -\frac{1}{2}\left(\frac{\partial p^{n+1}}{\partial x_i} - \frac{\partial p^n}{\partial x_i}\right), \tag{4}$$

$$\frac{\partial u_j^{n+1}}{\partial x_j} = 0. \tag{5}$$

The above formulation introduces a vortex sheet of strength $\mathcal{O}(\Delta t)^2$ at the boundaries which vanishes in the steady state. It is easy to see that v_i can be obtained from (3) by solving three scalar decoupled Helmholtz equations, while (u_i^{n+1}, p^{n+1}) require an additional Poisson equation obtained applying the divergence operator to (4).

We recall that since the velocity and pressure are decoupled from each other, the space discretizations for the velocity and pressure can be chosen independently, and they do not need to satisfy the Babuska–Brezzi condition [29]. Thus we have used equal order Legendre polynomials for both velocity and pressure. The pressure Poisson equation is solved with homogeneous Neumann boundary conditions on $p^{n+1} - p^n$.

3. The elliptic kernel

In this section we develop a spectral weak Legendre multi-domain algorithm for the solution of elliptic equation, representative of one of the scalar Helmholtz-like problems mentioned in the previous section. Let us consider the following problem:

$$\begin{aligned} &-\frac{\partial^2 u}{\partial x_j^2} + \alpha u = f \quad \text{in } \tilde{\Omega}, \\ &u = g_D \quad \text{on } \partial\tilde{\Omega}_D, \\ &\frac{\partial u}{\partial x_j} n_j = g_N \quad \text{on } \partial\tilde{\Omega}_N, \end{aligned} \tag{6}$$

with $\tilde{\Omega}$ an open connected set $\tilde{\Omega} \subset \mathbb{R}^3$, $\partial\tilde{\Omega} = \partial\tilde{\Omega}_D \cup \partial\tilde{\Omega}_N$, $\partial\tilde{\Omega}_D \cap \partial\tilde{\Omega}_N = \emptyset$, n_i the ith component of the outwarding normal on $\partial\tilde{\Omega}$, and $\alpha \geqslant 0$ a real constant. In the following, for the sake of brevity, we will only consider the homogeneous Dirichlet problem (i.e. $\partial\tilde{\Omega} = \partial\tilde{\Omega}_D$ and $g_D = 0$). The non-homogeneous case is straightforward in the weak collocation approach; the Neumann case is easily embodied in the multi-domain formulation, i.e. there is no conceptual nor practical difference between a connecting boundary and $\partial\tilde{\Omega}_N$ as it will be discussed later on.

Assuming the source term $f \in \mathbb{L}^2(\tilde{\Omega})$, the equivalent weak formulation of (6), is

$$\begin{cases} \text{find } u \in \mathbb{H}_0^1(\tilde{\Omega}) \\ \text{such that } a(u, v) = (f, v)_{\mathbb{L}^2(\tilde{\Omega})} \quad \forall v \in \mathbb{H}_0^1(\tilde{\Omega}), \end{cases} \tag{7}$$

where $\mathbb{H}_0^1(\tilde{\Omega})$ is the subspace of $\mathbb{H}^1(\tilde{\Omega})$ of the functions whose trace at the boundary is zero; $\mathbb{H}^1(\tilde{\Omega})$ is the space of functions belonging to $\mathbb{L}^2(\tilde{\Omega})$ such that their first order distributional derivatives belong to $\mathbb{L}^2(\tilde{\Omega})$ equipped with the scalar product

$$a(u,v)=\int_{\tilde{\Omega}}\left(\frac{\partial u}{\partial x_j}\frac{\partial v}{\partial x_j}+\alpha uv\right)\mathrm{d}\Omega\quad\forall u,v\in\mathbb{H}_0^1(\tilde{\Omega}) \tag{8}$$

and

$$(u,v)_{\mathbb{L}^2(\tilde{\Omega})}=\int_{\tilde{\Omega}}uv\,\mathrm{d}\Omega\quad\forall u,v\in\mathbb{L}^2(\tilde{\Omega}). \tag{9}$$

Suppose now that the domain $\tilde{\Omega}$ is partitioned into M_d non-overlapping subdomains $\tilde{\Omega}_i$

$$\overline{\tilde{\Omega}}=\cup_{i=1}^{M_d}\overline{\tilde{\Omega}}_i,\quad\tilde{\Omega}_i\cap\tilde{\Omega}_j=\emptyset\quad\text{for } i\neq j, \tag{10}$$

with $\overline{\tilde{\Omega}}_i$ a closed parallelepipedic domain.

Following the standard domain decomposition technique of variational problems [19], we define the interface Γ as follows:

$$\Gamma=(\tilde{\Omega}\setminus\tilde{\Omega}_0)\setminus\partial\tilde{\Omega}\quad\text{with }\tilde{\Omega}_0=\bigcup_{i=1}^{M_d}\tilde{\Omega}_i, \tag{11}$$

and introduce the additive decomposition of the solution of problem (7)

$$u=u_0+\tilde{u}. \tag{12}$$

In the above decomposition $u_0\in\mathbb{H}_0^1(\tilde{\Omega}_0)$ and $\tilde{u}\in\mathbb{H}_0^1(\tilde{\Omega})$ are solutions of the following problems:

$$\text{Problem P1}:\qquad a(u_0,v_0)=(f,v_0)_{\mathbb{L}^2(\tilde{\Omega})}\quad\forall v_0\in\mathbb{H}_0^1(\tilde{\Omega}_0), \tag{13}$$

$$\text{Problem P2}:\qquad a(\tilde{u},v)=(f,v)_{\mathbb{L}^2(\tilde{\Omega})}-a(u_0,v)\quad\forall v\in\mathbb{H}_0^1(\tilde{\Omega}). \tag{14}$$

The solution u_0 will deal with the interior unknowns of the various subdomains while $\tilde{u}$ will be related to the interface variables.

Let us assume the $x_3=z$-direction to be homogeneous. Denoting with L_z the periodic length in the z-direction and with Ω an arbitrary smooth two-dimensional region of $\mathbb{R}^2$, we can express the physical domain as $\tilde{\Omega}=\Omega\times[0,L_z]$. Furthermore, let us define $\tilde{\Omega}_i=\Omega_i\times[0,L_z]$ where Ω_i are closed rectangles, with dimension L_x and L_y in x- and y-direction, respectively, having either common sides or common vertices with each neighbor and $\Omega_0=\bigcup_{i=1}^{M_d}\Omega_i$. Following the blended Fourier and Legendre approximation [30], we represent each of the full three-dimensional scalar functions involved in Problem P1 and Problem P2 as follows:

$$u(x,y,z)=\sum_{k=-N_z/2}^{N_z/2-1}u^k(x,y)\mathrm{e}^{\mathrm{I}\beta kz}, \tag{15}$$

where $\beta=2\pi/L_z$ denotes the wave number and $\mathrm{I}=\sqrt{-1}$. Such a position allows us to reformulate both Problems P1 and P2 as a set of N_z uncoupled two-dimensional problems in terms of $u_0^k\in\mathbb{H}_0^1(\Omega_0)$ and $\tilde{u}^k\in\mathbb{H}_0^1(\Omega)$ as follows:

$$\text{Problem P1}:\qquad a^k(u_0^k,v_0)=(f^k,v_0)_{\mathbb{L}^2(\Omega)}\quad\forall v_0\in\mathbb{H}_0^1(\Omega_0), \tag{16}$$

$$\text{Problem P2}:\qquad a^k(\tilde{u}^k,v)=(f^k,v)_{\mathbb{L}^2(\Omega)}-a^k(u_0^k,v)\quad\forall v\in\mathbb{H}_0^1(\Omega) \tag{17}$$

in which

$$a^k(u,v)=\int_{\Omega}\left(\frac{\partial u}{\partial x_j}\frac{\partial v}{\partial x_j}+\epsilon^k uv\right)\mathrm{d}\Omega\quad\forall u,v\in\mathbb{H}_0^1(\Omega), \tag{18}$$

with $\epsilon^k = \alpha + (2\pi k/L_z)^2$. In the subsequent discussion, for the sake of clarity, we will drop out the superscript k.

Spatial discretization proceeds by restricting u_0 and $\tilde{u}$ to compatible finite dimensional spaces $\mathbb{X}^N \subset \mathbb{H}^1_0(\Omega_0)$ and $\tilde{\mathbb{X}}^N \subset \mathbb{H}^1_0(\Omega)$, respectively, and using appropriate quadrature to approximate the bilinear forms involved in (13) and (14).

We make use of the following notation: let us define the space

$$\mathbb{P}_{N,M_d}(\Omega) = \{\phi \in \mathbb{L}^2(\Omega) : \phi|_{\Omega_i} \in \mathbb{P}_N(\Omega_i)\}, \tag{19}$$

where $\mathbb{P}_N(\Omega_i)$ denotes the tensor product space of all polynomials of degree $\leqslant N_x$ in the x direction and $\leqslant N_y$ in the y direction. In what follows we assume, for the sake of clarity, that the pair (N_x, N_y) is equal for all subdomains. Having denoted with (ξ_k, η_l), $0 \leqslant k \leqslant N_x; 0 \leqslant l \leqslant N_y$, the $(N_x+1)(N_y+1)$ nodes of the Gauss–Lobatto–Legendre (GLL) integration formula in the reference domain $[-1,1]\times[-1,1]$, it is straightforward to define the pair (x_k^i, y_l^i), for each domain, by an affine transformation mapping of $[-1,1]\times[-1,1]$ onto $\overline{\Omega}_i$. Moreover, let $\gamma_{kl} = \gamma_k\gamma_l$ be the quadrature weights associated to the nodes (ξ_k, η_l), and $\omega_{kl}^i = \gamma_{kl} \cdot \mathrm{meas}(\Omega_i)/4$ the weights corresponding to domain Ω_i. With the above notations, following the spectral collocation technique, we define:

$$\mathbb{X}^N = \mathbb{H}^1_0(\Omega_0) \cap \mathbb{P}_{N,M_d}(\Omega),$$
$$\tilde{\mathbb{X}}^N = \mathbb{H}^1_0(\Omega) \cap \mathbb{P}_{N,M_d}(\Omega).$$

Therefore, problems (13) and (14) can be rewritten as follows:

$$\begin{cases} \text{Find } u_0^N \in \mathbb{X}^N \\ \text{such that } a_{\mathrm{GLL}}(u_0^N, v_0^N) = (f, v_0^N)_{\mathrm{GLL}} \quad \forall v_0^N \in \mathbb{X}^N, \end{cases} \tag{20}$$

$$\begin{cases} \text{Find } \tilde{u}^N \in \tilde{\mathbb{X}}^N \\ \text{such that } a_{\mathrm{GLL}}(\tilde{u}^N, v^N) = (f, v^N)_{\mathrm{GLL}} - a_{\mathrm{GLL}}(u_0^N, v^N) \quad \forall v^N \in \tilde{\mathbb{X}}^N, \end{cases} \tag{21}$$

where $a_{\mathrm{GLL}}(\cdot,\cdot)$ and $(\cdot,\cdot)_{\mathrm{GLL}}$ represent the Gauss–Lobatto–Legendre quadrature of the inner product in $\mathbb{H}^1(\Omega)$ and in $\mathbb{L}^2(\Omega)$, given by (8) and (9), respectively.

In the present paper we have chosen as basis for $\mathbb{P}_N(\Omega_i)$, the tensor product of the one-dimensional Gauss–Lobatto Lagrangian interpolant in both x and y directions. Thus, within each subdomain Ω_i, any function belonging to $\mathbb{X}^N$ and $\tilde{\mathbb{X}}^N$ can be represented in terms of the following basis:

$$\{h^k(x)h^l(y), \quad k = 1,\ldots,N_x-1, l = 1,\ldots,N_y-1\}, \tag{22}$$

$$\{h^k(x)h^l(y), \quad k = 0,\ldots,N_x, l = 0,\ldots,N_y\}, \tag{23}$$

where $h^k(x)$ and $h^l(y)$ are the one-dimensional Lagrangian interpolants in x and y directions, respectively. Taking into account the space basis definition (22) and owing to the exactness of the Gauss–Lobatto–Legendre integration formula, problem (20) becomes

$$\left[-\Delta u_0^{N,i}(x_k^i, y_l^i) + \epsilon u_0^{N,i}(x_k^i, y_l^i)\right]\omega_{kl}^i = f(x_k^i, y_l^i)\omega_{kl}^i \quad \forall (x_k^i, y_l^i) \in \Omega_i, \tag{24}$$
$$u_0^{N,i}(x_k^i, y_l^i) = 0 \quad \forall (x_k^i, y_l^i) \in \partial\Omega_i. \tag{25}$$

As far as problem (21) is concerned, the chosen span of $\tilde{\mathbb{X}}^N$ given by (23) implies the following algebraic formulation:

$$\left[-\Delta\tilde{u}^{N,i}(x_k^i, y_l^i) + \epsilon\tilde{u}^{N,i}(x_k^i, y_l^i)\right]\omega_{kl}^i = f(x_k^i, y_l^i)\omega_{kl}^i - \left[-\Delta u_0^{N,i}(x_k^i, y_l^i) + \epsilon u_0^{N,i}(x_k^i, y_l^i)\right]\omega_{kl}^i \quad \forall (x_k^i, y_l^i) \in \Omega_i, \tag{26}$$

$$u^{N,i}(x_k^i, y_l^i) = 0 \quad \forall (x_k^i, y_l^i) \in \partial\Omega_i \cap \partial\Omega, \tag{27}$$

$$\sum_{j=1}^{M_{kl}^i} \left\{ \omega_{kl}^j \Big[-\Delta\tilde{u}^{N,j}(x_k^i, y_l^i) + \epsilon \tilde{u}^{N,j}\big(x_k^i, y_l^i\big) \Big] + \zeta_{kl}^j \frac{\partial \tilde{u}^{N,j}}{\partial \mathbf{n}} \right.$$
$$\left. = f(x_k^i, y_l^i)\omega_{kl}^j - \omega_{kl}^j \Big[-\Delta u_0^{N,i}(x_k^i, y_l^i) + \epsilon u_0^{N,i}\big(x_k^i, y_l^i\big) \Big] - \zeta_{kl}^j \frac{\partial u_0^{N,j}}{\partial \mathbf{n}} \right\} \quad \forall (x_k^i, y_l^i) \in \partial\Omega_i \cap \Gamma, \tag{28}$$

where $\partial \cdot / \partial \mathbf{n}$ is the normal derivative, M_{kl}^i the number of subdomains sharing the point (x_k^i, y_l^i) with the domain Ω_i, and

$$\zeta_{kl} = \begin{cases} \gamma_k \cdot L_x/2 & \text{if } k = 0 \text{ or } N_x \quad \forall l = 0, \ldots, N_y, \\ \gamma_l \cdot L_y/2 & \text{if } l = 0 \text{ or } N_y \quad \forall k = 0, \ldots, N_x \end{cases} \tag{29}$$

having dropped the superscript j. Obviously, $M_{kl}^i = 4$ for interior corner configurations, and $M_{kl}^i = 2$ or $M_{kl}^i = 1$ for those subdomain setup involving Neumann boundary conditions; note that in case of Dirichlet boundary conditions, M_{kl}^i can either be zero or one.

Taking (24) into account, it follows that equation (26) can be rewritten as:

$$\Big[-\Delta\tilde{u}^{N,i}(x_k^i, y_l^i) + \epsilon \tilde{u}^{N,i}\big(x_k^i, y_l^i\big) \Big] \omega_{kl}^i = 0 \quad \forall (x_k^i, y_l^i) \in \Omega_i. \tag{30}$$

Problem (24) and (25) is nothing other than the solution of M_d decoupled elliptic problems (for each subdomain) with homogeneous boundary conditions, that can be efficiently and conveniently solved with the matrix diagonalization technique [31].

Concerning problem (30), (27) and (28), the elimination of the known boundary values leads to the following algebraic system:

$$\begin{bmatrix} \mathbf{H}_{11} & \ldots & \mathbf{0} & \mathbf{H}_{1\Gamma} \\ \ldots & \ldots & \ldots & \ldots \\ \mathbf{0} & \ldots & \mathbf{H}_{M_d M_d} & \mathbf{H}_{M_d \Gamma} \\ \mathbf{H}_{\Gamma 1} & \ldots & \mathbf{H}_{\Gamma M_d} & \mathbf{H}_{\Gamma\Gamma} \end{bmatrix} \begin{bmatrix} \mathbf{u}_1 \\ \ldots \\ \mathbf{u}_{M_d} \\ \mathbf{u}_\Gamma \end{bmatrix} = \begin{bmatrix} \mathbf{0} \\ \ldots \\ \mathbf{0} \\ \mathbf{q}_\Gamma \end{bmatrix} \tag{31}$$

in which we have denoted with: $\mathbf{u}_i$ the nodal values in Ω_i (only internal nodes) and $\mathbf{u}_\Gamma$ the interface values; $\mathbf{H}_{ii}$ the discretized Helmholtz operator on the subdomain Ω_i; $\mathbf{H}_{i\Gamma}$ the coupling between the unknowns defined in Ω_i and the interface Γ; $\mathbf{H}_{\Gamma i}$ the coupling between the unknowns defined on Γ and the subdomain Ω_i; $\mathbf{H}_{\Gamma\Gamma}$ the coupling among the unknowns belonging to Γ; $\mathbf{q}_\Gamma$ the source term depending on the interface values of u_0 and f, given by the r.h.s. of (28).

The block matrices $\mathbf{H}_{ii}$ are symmetric by construction as mentioned in [19]; also $\mathbf{H}_{i\Gamma}$ equals $\mathbf{H}_{\Gamma i}$ since they all come from the spectral discretization of an elliptic, coercive, regular, and uniform problem that is self-adjoint [32].

4. Solving the elliptic system

Elimination of the variables at interior nodes leads to following system (Schur complement):

$$\left(\mathbf{H}_{\Gamma\Gamma} - \sum_{i=1}^{M_d} \mathbf{H}_{\Gamma i} \mathbf{H}_{ii}^{-1} \mathbf{H}_{i\Gamma} \right) \mathbf{u}_\Gamma \equiv \mathbf{S}\mathbf{u}_\Gamma = \mathbf{g}_\Gamma. \tag{32}$$

The Schur complement problem (32), involving the interface values, can be solved either by direct method or by iterative procedure. For the class of problems we are concerned with, the construction and factorization of $\mathbf{S}$ is impractical both in terms of storage (matrix $\mathbf{S}$ is dense and large since it grows like $(M_d \times (N_x + N_y))^2$) and computational complexity. Thus iterative approaches not requiring the explicit construction of $\mathbf{S}$ are preferable. Although the condition number of the Schur complement matrix $\mathbf{S}$ is smaller than the condition number of the matrix involved in the original system (31), a preconditioner in the iterative procedure is imperative [33]. Since $\mathbf{S}$ is symmetric it's natural to consider the Conjugate Gradient (CG) method as the baseline solver. Alternatively one may prefer to apply a preconditioned version of CG (PCG) through the introduction of a suitable matrix $\mathbf{M}$. We recall that in PCG, or in the unpreconditioned version, the action of $\mathbf{S}$ onto $\mathbf{u}$ is computed through a global sum of matrix–vector products each of which is performed locally at subdomain level [34,35].

Together with the classical point Jacobi (PJ) and block Jacobi (BJ) preconditioner (like in [23]), we consider two preconditioners, belonging to the additive two level class, which can be written as the sum of two matrices taking into account local and global components:

$$\mathbf{M} = \mathbf{M}_{\text{glob}} + \mathbf{M}_{\text{loc}}. \tag{33}$$

This class of preconditioners has been successfully used in conjunction with finite elements and finite differences methods (see, among many others [36,35]). Depending upon the size of both $\mathbf{M}_{\text{glob}}$ and $\mathbf{M}_{\text{loc}}$ it may be convenient to invert and store $\mathbf{M}$ or to iteratively compute it.

Note that both the Point Jacobi and Block Jacobi preconditioners can be interpreted by means of (33) with $\mathbf{M}_{\text{glob}} = \mathbf{0}$, $\mathbf{M}_{\text{loc}} = \mathbf{M}_{\text{PJ}}$ and $\mathbf{M}_{\text{loc}} = \mathbf{M}_{\text{BJ}}$, respectively. In this paper we propose to use a similar technique for conforming spectral collocation multi-domain methods.

Let us begin with some nomenclature. Let n_{e} be the total number of edges and n_{v} the number of vertices. We define, out of the set of interface collocation points belonging to Γ, three sub-sets E_k, $\dot{E}_k$ ($k = 1, \ldots, n_{\text{e}}$) and V_l. The set E_k contains all nodes belonging to the kth edge, $\dot{E}_k$ all but the end nodes of the kth edge, and V_l ($l = 1, \ldots, n_{\text{v}}$) the individual vertices. Assuming for the sake of clarity $N_x = N_y = N$, the dimension of the space where the Schur complement is defined ($\mathbb{U}$) is $n_{\text{s}} = n_{\text{e}} \times (N-2) + n_{\text{v}}$ (i.e. $\mathbb{U} \subseteq \mathbb{R}^{n_{\text{s}}}$). Let us further introduce a coarse space $\mathbb{U}_0$, a q-dimension subspace of $\mathbb{U}$ (with $q \leqslant n_{\text{s}}$) and a restriction operator $\mathbf{R}_0$:

$$\mathbf{R}_0 : \mathbf{u} \in \mathbb{U} \subseteq \mathbb{R}^{n_{\text{s}}} \rightarrow \mathbf{u}_0 \in \mathbb{U}_0 \subseteq \mathbb{R}^q. \tag{34}$$

With the above definitions, the global preconditioner $\mathbf{M}_{\text{glob}}$ can be written in general terms as

$$\mathbf{M}_{\text{glob}} = \mathbf{R}_0^{\text{T}} \mathbf{A}_0^{-1} \mathbf{R}_0, \tag{35}$$

where

$$\mathbf{A}_0 = \mathbf{R}_0 \mathbf{S} \mathbf{R}_0^{\text{T}}. \tag{36}$$

Depending on the particular choice of both $\mathbb{U}_0$ and $\mathbf{R}_0$, several global preconditioners can be built. In the present paper we have chosen as $\mathbb{U}_0$ the vertex based coarse space (whose dimension q is the number of vertices n_{v}) and as $\mathbf{R}_0$ the flat restriction operator [37]. Such a global preconditioner, introduced in the finite difference and finite element context by Carvalho et al. [37], is closely related to the global part of the preconditioner first introduced by Bramble et al. [36], in which the matrix $\mathbf{A}_0$ represents the coarse grid approximation of the original elliptic operator. It has been shown [37] that the global coupling expressed by (35) together with definition (36) offers performances similar to those of the original global preconditioner of Bramble et al. [36] and furthermore it is characterized by a simpler algebraic structure and is thus well suited for parallel implementations.

As far as the local part is concerned, let us decompose the $\mathbb{U}$ space in a set of p subspaces

$$\mathbb{U} = \sum_{i=1}^{p} \mathbb{U}_i, \tag{37}$$

each of which with dimension q_i ($q_i \leqslant n_s$), and let $\mathbf{R}_i$ be the canonical point wise restriction operator of the nodal values defined on $\mathbb{U}_i$. Its transpose $\mathbf{R}_i^T$ prolongates the functional values in $\mathbb{U}_i$ to the space $\mathbb{U}$. The prolongation effectively corresponds to extend by zeros $n_s - q_i$ values. A general local preconditioner can be expressed as follows:

$$\mathbf{M}_{loc} = \sum_{i=1}^{p} \mathbf{R}_i^T \mathbf{A}_i^{-1} \mathbf{R}_i, \tag{38}$$

in which $\mathbf{A}_i = \mathbf{R}_i \mathbf{S} \mathbf{R}_i^T$. As before, depending on the choice of the subspace $\mathbb{U}_i$ several local preconditioners can be built.

Similarly to Bramble et al. [36], we build a local edge preconditioner associating each subspace $\mathbb{U}_i$ to each edge set $\dot{E}_k$ and each vertex set V_l (i.e. $p = n_e + n_v$):

$$\mathbf{M}_{loc} = \mathbf{M}_E = \sum_{k=1}^{n_e} \mathbf{R}_k^T \mathbf{A}_k^{-1} \mathbf{R}_k + \sum_{l=1}^{n_v} \mathbf{R}_l^T \mathbf{A}_l^{-1} \mathbf{R}_l. \tag{39}$$

Such a preconditioner is the well-known Block Jacobi and it is therefore efficiently parallelizable; it accounts for the interaction among all nodes belonging to the same edge interface [38]. The last term of the r.h.s. of (39) corresponds to a simple diagonal scaling at the equations associated to the vertices V_l. The major shortcoming of such a local preconditioner relies in its impossibility to manage nodes belonging to all those edges which converge into a single vertex.

In order to overcome the above deficiency let us associate each subspace $\mathbb{U}_i$ to the enlarged edge set E_k, and build the vertex–edge preconditioner

$$\mathbf{M}_{loc} = \mathbf{M}_{VE} = \sum_{k=1}^{n_e} \mathbf{R}_k^T \mathbf{A}_k^{-1} \mathbf{R}_k. \tag{40}$$

Such a preconditioner shares similarities with the Vertex-Space (VS) preconditioner introduced by Smith [35] in the context of Finite Element methods, and by Casarin [38] and Pavarino and Widlund [25] in the context of spectral element discretizations. Unlike Smith who considers in an additive way the effects of both vertices and edges, we merge them into a single subspace.

Let us simply remark that, similarly to the residual construction in the PCG procedure, both the local and global components of $\mathbf{M}$ are gathered through a sum of local matrix–matrix products [37].

In the next section, in the framework of the weak-Legendre multi-domain discretization, we compare the performances of the Point Jacobi, Block Jacobi preconditioners and the following additive two level preconditioners:

$$\mathbf{M}_{ES} = \mathbf{M}_{glob} + \mathbf{M}_E, \quad \mathbf{M}_{VS} = \mathbf{M}_{glob} + \mathbf{M}_{VE} \tag{41}$$

with those of PDM.

The PDM provides a solution that approximates the exact one with the spectral accuracy. Moreover, owing to the piecewise-polynomial well conditioned basis used in the Galerkin formulation of the interface Steklov–Poincaré equation, it leads to a linear system whose coefficients matrix is symmetric, with condition number independent on the degree of the polynomials and mildly dependent on the number the subdomains [19].

5. Results

Hereafter we present numerical results for three test problems which clearly demonstrate the potential of the method compared to [19]. We have carefully attempted to objectively evaluate the performances of the methods reporting, whenever possible, details concerning the implementations. As anticipated in Section 2 the emphasis of the paper is centered on the elliptic kernel; however, and for sake of completeness, a few results are also given for the Navier–Stokes equations.

5.1. Elliptic equations

As already mentioned the elliptic kernel (of Helmholtz and Poisson type) constitutes the core of the Navier–Stokes solver; it is thus natural that we first concentrate on elliptic problems arising from the setup of practical fluid dynamics interest. We have already discussed the fact that the disparity in length scales characterizing many, if not all of the above processes, requires adequate mesh resolution, a task that is more easily accomplished through a proper control of the number of subdomains and the polynomial degree of the spectral approximation. Thus we have investigated the effects of both procedures, separately, so that merits and drawbacks of the available methods could be more clearly highlighted.

5.1.1. The isotropic case

In this subsection, we present some results concerning the solution of the Helmholtz equation

$$-\Delta u + \epsilon u = f \quad \text{in } \Omega = [0,1] \times [0,1], \tag{42}$$

with $\epsilon = 1$, and

$$f = \mathrm{e}^{x+y}[(8\pi^2 - 1)\cos(2\pi x)\cos(2\pi y) + 4\pi \sin(2\pi(x+y))] \tag{43}$$

for which the analytic solution

$$u(x,y) = \mathrm{e}^{x+y}\cos(2\pi x)\cos(2\pi y) \tag{44}$$

exists.

We have considered both Dirichlet and Neumann boundary conditions of either homogeneous or inhomogeneous type; however, for sake of brevity and in light of the fact that the achievements of the study are not affected by the kind of boundary condition adopted, we shall present a systematic comparison of the performances of several elliptic solvers for a single set of boundary conditions (of inhomogeneous Dirichlet type). The domain Ω is split in M_d equally sized subdomains so that the number of subdomains in the x and y direction equals $\sqrt{M_d}$. In addition the polynomial degree of the approximation is such that $N_x = N_y = N$. Note that the number of internal cross points is considerable and grows like $(\sqrt{M_d} - 1)^2$.

Before all let us demonstrate that the error is exponentially decaying when the number of Legendre modes is increased.

In Table 1 we have reported the $\mathbb{H}^1$ norm of the error for several (N, M_d) pairs ($4 \leqslant N \leqslant 10$ and $4 \leqslant M_d \leqslant 121$). As expected the error is squared (or more) when the number of modes N is doubled.

It is straightforward to verify that the rate of convergence with M_d is algebraic (power law) with an exponent that increases from 1.96 to 3.97 when N is varied between 4 and 8. We remark that within three significant digits the error looks to decay like $\sim M_d^{-N/2}$.

Fig. 1 shows the condition number κ versus both the number of Legendre modes N (for $M_d = 25$) and the number of subdomains M_d (for $N = 6$). The test matrix investigated is actually larger, with N and M_d ranging from 4 to 10, and 4 to 121, respectively; however, for sake of brevity only two cases are presented; data can be made available to potentially interested readers. Let us begin observing that the growth of κ of

Table 1
$\mathbb{H}^1$ norm of the error for isotropic model problem

M_d	N			
	4	6	8	10
4	3.13×10^{-1}	2.75×10^{-3}	1.16×10^{-5}	5.38×10^{-8}
9	6.79×10^{-2}	4.07×10^{-4}	1.41×10^{-6}	3.14×10^{-9}
16	2.19×10^{-2}	7.41×10^{-5}	1.47×10^{-7}	1.91×10^{-10}
25	9.14×10^{-3}	1.97×10^{-5}	2.51×10^{-8}	2.11×10^{-11}
64	1.45×10^{-3}	1.18×10^{-6}	5.97×10^{-10}	7.69×10^{-13}
100	6.04×10^{-4}	3.16×10^{-7}	1.00×10^{-10}	1.04×10^{-12}
121	4.15×10^{-4}	1.79×10^{-7}	4.70×10^{-11}	8.38×10^{-13}

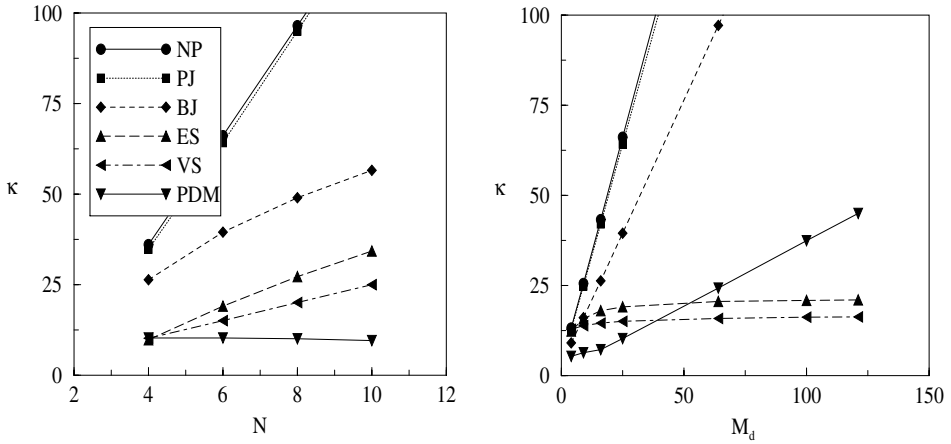

Fig. 1. Condition number versus the number of Legendre modes for $M_d = 25$ (left) and versus the number of subdomains for $N = 6$ (right); isotropic model problem.

the unpreconditioned (NP) Schur matrix is practically linear both with the number of subdomains M_d and Legendre modes N. This is a consequence of the moderate number of points N; in fact increasing N up to 40 ($M_d = 4$, results not shown herein) we recover the quadratic dependence of [33]. There are no appreciable improvements with the PJ preconditioner.

This is unfortunate given the very modest computational overhead required to build (and store) the PJ preconditioner. We are not aware of any general estimate of the functional dependence of κ with both N and M_d, but, in view of the appealing behavior of the VS preconditioner we conjecture that the lack of transmission information in presence of numerous cross points among subdomains is the main reason of the poor performance of this and other local preconditioners.

Moving on to the performance of the block Jacobi preconditioner, we note that the rate of increase of κ with N, in accordance with the theoretical estimates of Casarin [38], is less than linear. Conversely κ grows linearly with M_d. There is a considerable improvement, instead, with the ES preconditioner; not only are the magnitudes of κ reduced, but, most important, there is a clear tendency towards an asymptotic value when the number of subdomains is increased.

The main difference between the ES and VS preconditioners is an additional flattening of the condition number with M_d and a reduction in the "asymptotic value". The growth of κ with N appears to closely follow the theoretical estimates of [25,26] ($\kappa \leqslant (1 + log(N))^2$), although a significantly larger N would be needed to clearly ascertain this matter.

Also, the independence of the condition number upon the number of subdomains is similar to the one documented by numerical experiments in [38]. The PDM shows instead a linear growth with M_d. We note that the well conditioned basis yielding a convergence rate independent of N prove effective also with M_d, since the VS algorithm required as many as 70 subdomains solves to overwhelm the PDM when $N = 10$ (results not shown herein). However, when $N = 6$ the break-even point reduces to $M_d = 40$. Thus while the PDM is optimal with respect to the number of Legendre modes N and mildly dependent upon the number of subdomains M_d, the opposite is true for the vertex space algorithm. As concerns the optimal bound of the overlapping Schwarz method with respect to both M_d and N derived in [27], let us observe that the generous overlap needed to achieve the above theoretical estimate implies a larger computational cost compared to both the PDM and the two level preconditioners.

As a final remark we wish to underline the fact that, in the isotropic case, the condition numbers are all comparable and moderate, i.e. $\mathcal{O}(10^2)$. Thus, a direct solution procedure [39] is possible when $M_d \times N < \mathcal{O}(10^4)$. Indeed for elliptic problems with repeated right-hand sides and constant ϵ, it is recommendable to compute and store the LU factors. For three-dimensional problems the situation is more involved because of the storage constraints associated with the Fourier expansion (we have to store $N_z/2$ operators, since the Helmholtz coefficient ϵ depends on the Fourier mode).

Although the above results seem to suggest a substantial equivalence among the different procedures, we shall show in the next section that the presence of anisotropy may drastically change the scenario.

5.1.2. The anisotropic case

In the previous section we have investigated the effects of both the number of subdomains and Legendre modes on the condition of the algebraic system (32) for a model problem. In particular the number of subdomains was increased in an isotropic fashion, i.e. at each refinement stage the size of the corresponding elements differed by a scaling factor solely. This is the exception rather than the rule in fluid dynamics applications. Thus in this section we have concentrated on an anisotropic geometric configuration which is of relevance in a practical engineering problem.

The computational domain is representative of a rib roughened channel used as a cooling device inside the nozzle guide vanes of the last generation gas turbines. As for the previous model problem we have solved Eq. (42) with $\epsilon = 1$ and the source term f given by

$$f = \left[\left(\frac{2\pi}{L_x} \right)^2 + \left(\frac{2\pi}{L_y} \right)^2 + 1 \right] \cos\left(\frac{2\pi x}{L_x} \right) \cos\left(\frac{2\pi y}{L_y} \right), \tag{45}$$

so that the analytical solution is

$$u(x,y) = \cos\left(\frac{2\pi}{L_x} x \right) \cos\left(\frac{2\pi}{L_y} y \right). \tag{46}$$

The computational domain consists of a square rib $[0,\ell] \times [0,\ell]$ with $\ell = 0.6$ placed at the lower wall of a square channel $[0,L] \times [0,L]$ with $L = 6.0$, and thus $L/\ell = 10$.

We have considered four different partitions of the physical domain Ω with increasing number of subdomains (viz. $M_d = 5$, 22, 51, 92); the sizes of the subdomains were adjusted so to enhance the wall resolution (see Fig. 2). Note that the anisotropy associated to the above domain partitioning expressed in terms of the maximum and minimum aspect ratios over the subdomains and summarized in Table 2 is considerable. For each of these four configurations we have increased the polynomial degree of the approximation from 4 to 14 ($N = 4$, 6, 8, 10, 12, 14). As before $N_x = N_y = N$.

Table 3 reports the condition number of the unpreconditioned system for the four configurations described above, as a function of the Legendre modes N. The almost linear growth of κ with N is confirmed also in presence of considerable anisotropies.

We note that the effect of the anisotropy in terms of augmented spreading of the maximum to minimum eigenvalue ratio is considerable so that when M_d is $\mathcal{O}(100)$, κ becomes $\mathcal{O}(10^4)$ (to be compared with the corresponding values of the isotropic cases).

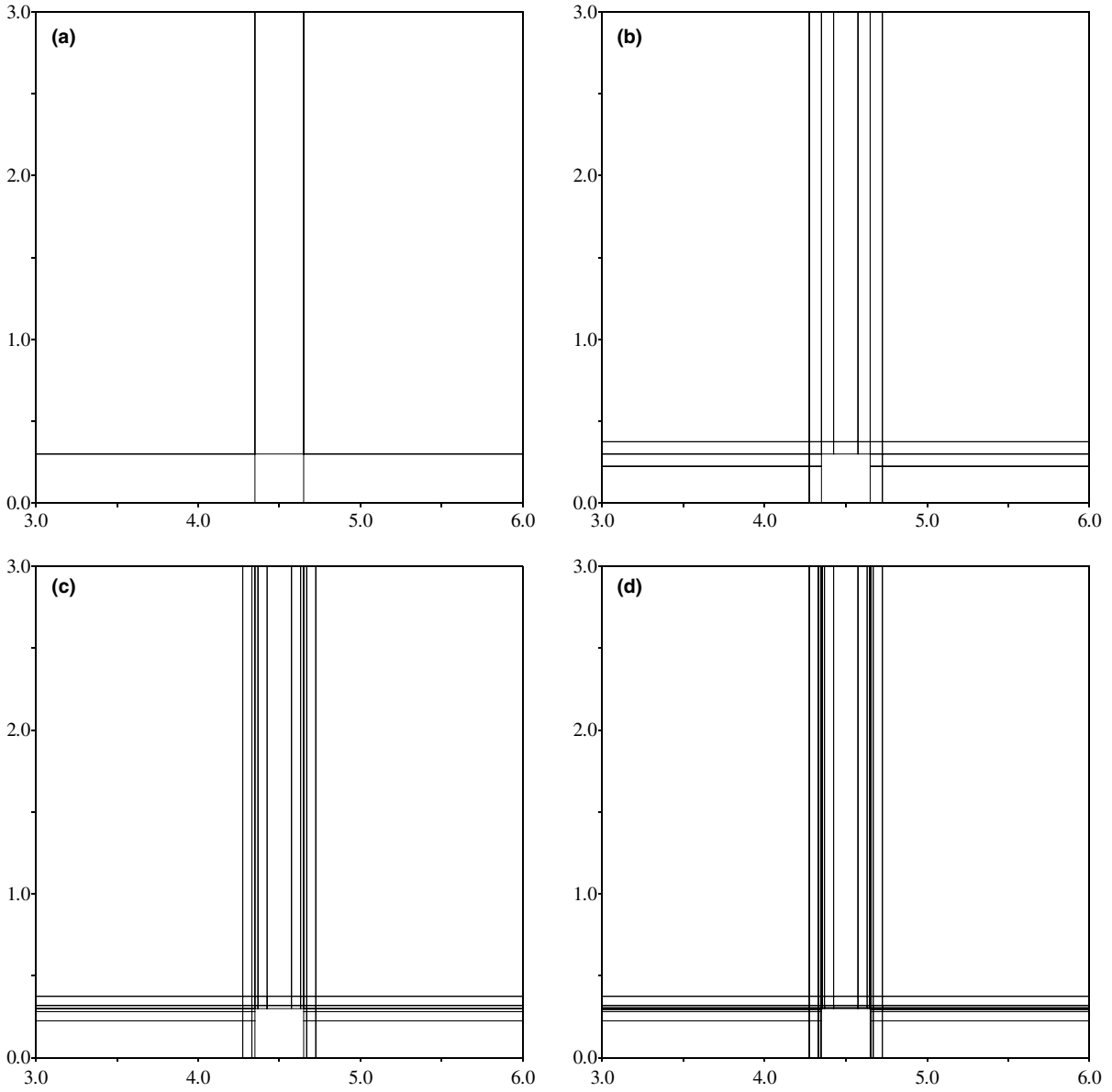

Fig. 2. Subdomain partition for anisotropic model problem; shown is one half of the computational domain: (a) $M_d = 5$, (b) $M_d = 22$, (c) $M_d = 51$, (d) $M_d = 92$.

Table 2
Maximum and minimum aspect ratios for anisotropic model problem

Total number of subdomains	5	22	51	92
Max. aspect ratio	4.50	17.0	68.0	272
Min. aspect ratio	1.1×10^{-1}	2.8×10^{-2}	7.1×10^{-3}	1.8×10^{-3}
Min. wall normal distance	1.15×10^{-1}	3.05×10^{-3}	8.13×10^{-4}	2.00×10^{-4}

Table 4, reporting the condition number of the point Jacobi preconditioner, shows that its efficiency is remarkable. In fact not only is κ more than halved for all values of N when $M_d = 51$ and $M_d = 92$, but in certain cases it even proves superior compared to the PDM.

Moving from the point version of the preconditioner to the block one determines significant improvements as evident from Table 5. This is interesting since it is the highest level preconditioner with local, on a subdomain basis, characteristics which is an appreciable feature in view of parallel applications.

Tables 6 and 7 report the performances of the ES and VS algorithms. There is a fair improvement, compared to the BJ preconditioner which in some instances (i.e. $M_d = 92$ and $N = 14$) may add up to 50%. For the most challenging case, viz. $M_d = 92$, the VS seems to have reached a remarkable, nearly independent from N behavior. All of the above three mentioned methods are clearly superior to what we consider our challenger, the PDM, whose performances are illustrated in Table 8. Let us first remark that in presence of anisotropy the PDM does not show an optimal behavior neither with M_d, nor with N (!). This is more evident from Fig. 3 where the data discussed above are compared on a graphic basis as a function of N for $M_d = 51$ (left figure), and as a function of M_d for $N = 8$ (right figure).

We wish to conclude this section drawing the reader's attention on the almost two order of magnitudes reduction of κ attainable with the VS preconditioner for an anisotropic configuration of engineering relevance.

Table 3
Condition number of the non-pre-conditioned (NP) Schur complement matrix; anisotropic model problem

M_d	N					
	4	6	8	10	12	14
5	7.51×10^{0}	1.42×10^{1}	2.06×10^{1}	2.74×10^{1}	3.44×10^{1}	4.16×10^{1}
22	1.52×10^{2}	2.58×10^{2}	3.68×10^{2}	4.81×10^{2}	5.96×10^{2}	7.12×10^{2}
51	1.50×10^{3}	2.60×10^{3}	3.73×10^{3}	4.87×10^{3}	6.02×10^{3}	7.17×10^{3}
92	1.07×10^{4}	1.85×10^{4}	2.66×10^{4}	3.48×10^{4}	4.31×10^{4}	5.13×10^{4}

Table 4
Condition number of the point Jacobi (PJ) pre-conditioned Schur complement matrix; anisotropic model problem

M_d	N					
	4	6	8	10	12	14
5	7.14×10^{0}	1.35×10^{1}	1.92×10^{1}	2.47×10^{1}	3.00×10^{1}	3.51×10^{1}
22	1.08×10^{2}	1.73×10^{2}	2.21×10^{2}	2.62×10^{2}	2.99×10^{2}	3.33×10^{2}
51	5.95×10^{2}	1.06×10^{3}	1.39×10^{3}	1.64×10^{3}	1.84×10^{3}	2.00×10^{3}
92	2.75×10^{3}	5.13×10^{3}	6.99×10^{3}	8.48×10^{3}	9.71×10^{3}	1.07×10^{4}

Table 5
Condition number of the block Jacobi (BJ) pre-conditioned Schur complement matrix; anisotropic model problem

M_d	N					
	4	6	8	10	12	14
5	5.42×10^0	8.33×10^0	1.09×10^1	1.31×10^1	1.51×10^1	1.70×10^1
22	6.69×10^1	8.08×10^1	9.02×10^1	9.82×10^1	1.05×10^2	1.11×10^2
51	3.63×10^2	4.72×10^2	5.20×10^2	5.46×10^2	5.63×10^2	5.77×10^2
92	1.67×10^3	2.26×10^3	2.56×10^3	2.74×10^3	2.85×10^3	2.93×10^3

Table 6
Condition number of the edge space (ES) pre-conditioned Schur complement matrix; anisotropic model problem

M_d	N					
	4	6	8	10	12	14
5	1.03×10^1	1.73×10^1	2.33×10^1	2.83×10^1	3.27×10^1	3.67×10^1
22	6.56×10^1	7.37×10^1	9.54×10^1	1.17×10^2	1.35×10^2	1.49×10^2
51	3.33×10^2	3.77×10^2	4.04×10^2	4.22×10^2	4.35×10^2	4.48×10^2
92	1.47×10^3	1.71×10^3	1.88×10^3	1.99×10^3	2.08×10^3	2.14×10^3

Table 7
Condition number of the vertex space (VS) pre-conditioned Schur complement matrix; anisotropic model problem

M_d	N					
	4	6	8	10	12	14
5	8.26×10^0	8.74×10^0	1.21×10^1	1.53×10^1	1.82×10^1	2.09×10^1
22	7.10×10^1	7.43×10^1	7.82×10^1	8.16×10^1	8.46×10^1	8.74×10^1
51	3.41×10^2	3.34×10^2	3.48×10^2	3.59×10^2	3.67×10^2	3.73×10^2
92	1.46×10^3	1.41×10^3	1.47×10^3	1.52×10^3	1.56×10^3	1.59×10^3

Table 8
Condition number of the PDM; anisotropic model problem

M_d	N					
	4	6	8	10	12	14
5	7.83×10^0	1.11×10^1	1.29×10^1	1.40×10^1	1.47×10^1	1.52×10^1
22	1.28×10^2	1.63×10^2	1.75×10^2	1.81×10^2	1.85×10^2	1.88×10^2
51	9.36×10^2	1.19×10^3	1.28×10^3	1.31×10^3	1.33×10^3	1.34×10^3
92	5.69×10^3	7.39×10^3	8.15×10^3	8.57×10^3	8.83×10^3	8.99×10^3

5.2. Direct and large eddy simulations of turbulent channel flow

This section deals with DNS and LES of fully developed turbulent channel flow at a Reynolds number of 180, based on friction velocity $u_\tau = \sqrt{\tau_w/\rho}$ and half channel height h, τ_w being the wall shear stress and ρ the fluid density. The idea is to validate the ability of the method in dealing with highly anisotropic subdomains, i.e. with aspect ratios of order 100, which are necessary to fully resolve the persistent and energetic

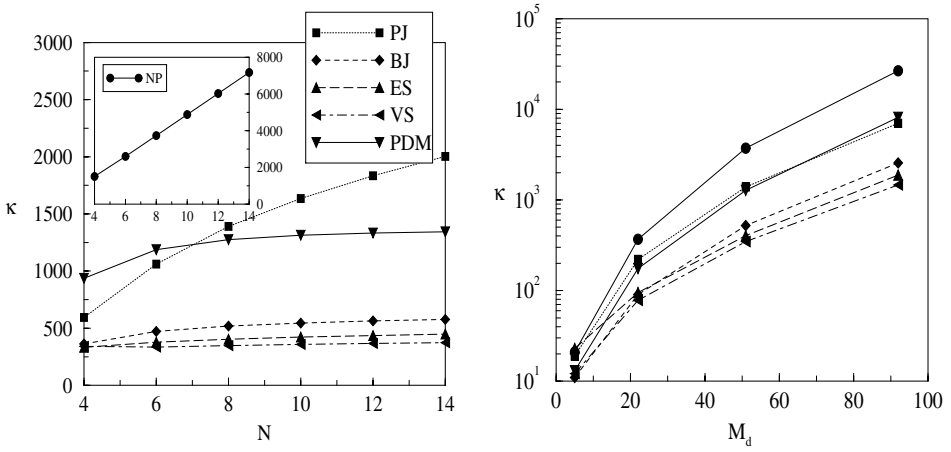

Fig. 3. Condition number versus the number of Legendre modes for $M_d = 51$ (left) and versus the number of subdomains for $N = 8$ (right); anisotropic model problem.

coherent near wall structures responsible for most of the turbulence production. The geometric environment has been purposely simplified to reduce the computational costs associated with three-dimensional unsteady direct simulations over bluff bodies. However, the physical domain partitioning strategy was devised in order to both maintain a significant number of interior corner points (whose presence affects to a great deal the elliptic kernel efficiency), and preserve the correct near wall resolution.

This model problem has received considerable attention over the past two decades, and many progresses in the understanding of wall turbulence have been achieved thanks to the numerical and experimental contributions. Thus, reference numerical and experimental data are available. Our DNS shall be compared with the data of Moser et al. [4] who have slightly changed the setup of the first celebrated channel flow DNS of Kim et al. [1]. The LES, which employed the widely used dynamic model of Germano et al. [40], as modified by Lilly [41], has been designed to have considerable more grid anisotropy compared to the DNS. Specifically, the normal to the wall resolution has been left unchanged, while the streamwise and spanwise resolutions were, roughly speaking, halved. The numerical method pertaining to the DNS case has been described in Section 2; the LES equations differ from the DNS ones for the presence of a highly non-linear elliptic term related to the subgrid stress tensor which is lumped in the non-linear operator $\mathcal{N}$ and treated explicitly, for sake of simplicity.

The channel size is identical to the one of Moser et al. [4], viz. $4\pi h \times 2h \times 2\pi$ in the streamwise, normal to the wall and spanwise directions, respectively. Those dimensions were demonstrated sufficient for the flow to be uncorrelated at the largest separation distance in the two homogeneous directions [4]. The DNS and LES resolutions are detailed in inner coordinates in Table 9. The normal to the wall subdomains partitioning strategy has been designed to enhance the resolution of the turbulent coherent wall structures, while uniform streamwise subdomains arrangement has been adopted. Present resolution is comparable to the one of reference [4]. The Navier–Stokes results were obtained on a Linux Box SMP dual PIII 750 MHZ machine, with a code written in f90.

As before, Table 10 details the condition number and the iterations required to converge a single spanwise mode ($k = 0$) of the Helmholtz problem arising from the solution of the streamwise velocity component. Compared are the performance of the VS and the PDM algorithm for both DNS and LES grid systems. The high anisotropy is found to play an important role, since the VS preconditioner always overwhelms the PDM in agreement with the results of Tables 7 and 8.

Table 9
Grids details for DNS and LES of turbulent channel flow

	DNS	LES
M_d	16×8	6×8
N	12	12
N_z	128	64
$M_d \times N \times N \times N_z$	2.4×10^6	4.4×10^5
Max. aspect ratio	16.7	44.4
$\Delta x^+_{\min}$	3.83	9.78
$\Delta x^+_{\max}$	26.98	69.87
$\Delta y^+_{\min}$	0.23	0.22
$\Delta y^+_{\max}$	10.79	10.48
Δz^+	5.9	11.47

Table 10
Conjugate gradient iterations and condition numbers for elliptic kernel (turbulent channel flow)

	LES		DNS	
	N_{iter}	κ	N_{iter}	κ
PDM [19]	136	174.20	76	56.61
VS preconditioner	82	50.98	54	40.62

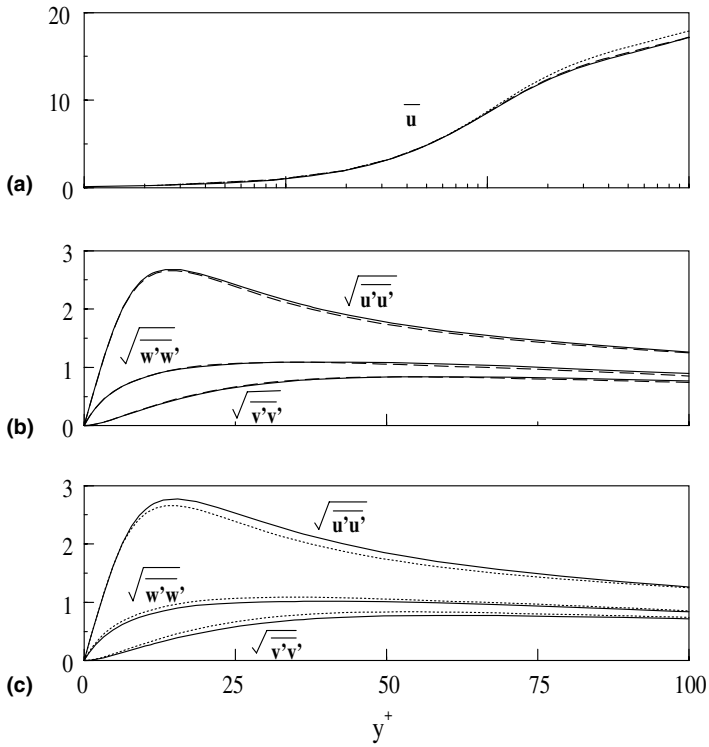

Fig. 4. Velocity profiles (a) and turbulence intensities (b) and (c); — Moser et al. [4]; present results: - - - DNS, ⋯ LES.

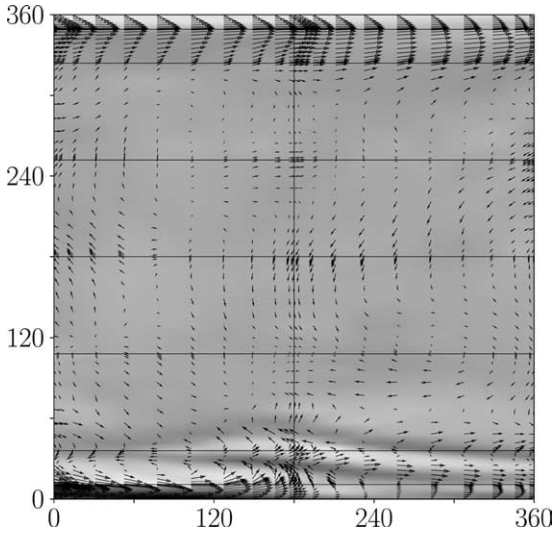

Fig. 5. Equilibrium turbulent channel flow; instantaneous velocity fluctuations superposed to spanwise vorticity shaded contours in an x–y plane.

The data are obtained processing 50 nearly independent fields separated in time by $0.1t^+$, where $t^+ = tu_\tau/h$. The time steps are $\Delta t^+ = 0.09 \times 10^{-3}$ and 0.15×10^{-3}, for the DNS and LES, respectively. The initial velocity field has been created superposing to a logarithmic distribution random noise with a prescribed standard deviation. The steady state is identified by a constant time averaged wall shear stress, and by a quasi-periodic turbulent kinetic energy.

Fig. 4 compares the present DNS and LES results with the reference DNS data of Moser et al. [4] obtained with a spectral single domain Chebyshev–Fourier–Fourier solver. The agreement between the two DNS calculations is, as expected, very good despite the slightly different resolutions both in wall normal and streamwise directions. Likewise the LES data agree well with the DNS distributions. We recall that, thanks to the flexibility of the multi-domain solver, the wall layer can be easily resolved, without increasing remarkably the computational cost.

In Fig. 5 an instantaneous snapshot of the spanwise vorticity fluctuations, obtained processing one of the DNS data set, is shown; superposed are the vectors of the fluctuating velocity components (i.e. time and space averaged values have been subtracted from instantaneous values). The spatial coordinates are represented in terms of wall values. The smoothness of the vorticity field in regions of high instantaneous shear is a clear indication that all turbulent scales are properly resolved.

6. Conclusions

We have presented a preconditioned multi-domain algorithm based on the iterative solution of the Schur complement matrix and applied it to the elliptic kernels arising from the spectrally collocated discretization of the incompressible Navier–Stokes equations in three space dimensions with one homogeneous direction. The technique allows for efficient numerical solutions of the operators in complex geometries consisting of a collection of non-overlapping rectangular subdomains. Both single and two level preconditioners are considered in simple and complex geometries characterized by remarkable anisotropies. While the former prove reasonably effective in the isotropic model problem, the latter are shown to be necessary whenever the subdomain aspect ratios are large. More specifically and with reference to the two level preconditioners,

both edge and vertex space algorithms prove effective in decreasing the condition number of the original system, so much that, for sufficiently large number of subdomains they outperform the PDM.

The method is shown to be nearly optimal in terms of asymptotic condition number behavior in a double path of refinement strategy, i.e. whenever both the number of Legendre modes and the number of subdomains are significantly increased. Therefore, there is little degradation of the performance when the number of interior corners is strongly increased.

The whole procedure is demonstrated to be particularly well suited for engineering applications in the fields of direct and large eddy simulations of turbulence.

References

[1] J. Kim, P. Moin, R. Moser, Turbulence statistics in fully developed channel flow at low Reynolds number, J. Fluid Mech. 177 (1987) 133–166.
[2] P.R. Spalart, Direct numerical simulation of turbulent boundary layer up $Re_\theta = 1410$, J. Fluid Mech. 187 (1988) 61–97.
[3] M. Rai, P. Moin, Direct numerical simulation of transition and turbulence in a spatially evolving boundary layer, J. Comput. Phys. 109 (1993) 169–192.
[4] R. Moser, J. Kim, N. Mansour, Direct numerical simulation of turbulent channel flow up $Re = 590$, Phys. Fluids 11 (4) (1999) 1938–1944.
[5] X. Wu, R. Jacobs, J. Hunt, P. Durbin, Simulation of boundary layer transition induced by periodically passing wakes, J. Fluid Mech. 398 (1999) 109–153.
[6] J. Jiménez, R.D. Moser, Large-eddy simulations where are we and what can we expect?, AIAA J. 38 (2000) 605–612.
[7] P. Sagaut, Large Eddy Simulation for Incompressible Flows. An Introduction, Springer, Berlin, 2001.
[8] J.M. Wallace, H. Eckelmann, R.S. Brodkey, The wall region in turbulent shear flow, J. Fluid Mech. 54 (1972) 39–48.
[9] B. Smith, P. Bjorstad, W. Gropp, Domain Decomposition, Cambridge University Press, New York, 2000.
[10] A. Quarteroni, A. Valli, Domain Decomposition Methods for Partial Differential Equations, Oxford University Press, Oxford, 2000.
[11] A.T. Patera, A spectral element method for fluid dynamics: laminar flow in a channel expansion, J. Comput. Phys. 54 (1984) 468–488.
[12] Y. Maday, A.T. Patera, Spectral element methods for the Navier–Stokes equations, in: A.K. Noor, J.T. Oden (Eds.), State-of-the-Art Surveys in Computational Mechanics, ASME, New York, 1989, pp. 71–143.
[13] R. Henderson, G. Karniadakis, Unstructured spectral element methods for simulation of turbulent flows, J. Comput. Phys. 122 (1995) 191–217.
[14] H.M. Tufo, P.F. Fisher, Tera-scale spectral element algorithms and implementations, in: Proceedings of the ACM/IEEE SC99 Conference on High Performance Networking and Computing, IEEE Computer Society, 1999, pages CD-Rom.
[15] H.M. Tufo, P.F. Fisher, Fast parallel direct solvers for coarse-grid problems, J. Parallel Distrib. Comput. 61 (2001) 151–177.
[16] E.M. Rønquist, A domain decomposition method for elliptic boundary value problems: application to unsteady incompressible fluid flow, in: D.E. Keyes, T.F. Chan, G. Meurant, J.S. Scroggs, R.G. Voigt (Eds.), Proceedings of the Fifth Conference on Domain Decomposition Methods for Partial Differential Equations, SIAM, Philadelphia, 1992, pp. 545–557.
[17] E.M. Rønquist, A domain decomposition solver for three-dimensional steady free surface flows flows, in: M. Espedal, P. Bjorstad, D.E. Keyes (Eds.), Domain Decomposition 9 Proceedings, Wiley, New York, 1998, pp. 792–801.
[18] S.A. Orszag, Spectral methods for problems in complex geometries, J. Comput. Phys. 37 (1980) 70–92.
[19] P. Gervasio, E. Ovtchinnikov, A. Quarteroni, The spectral projection decomposition method for elliptic equations in two dimensions, SIAM J. Numer. Anal. 4 (1997) 1616–1639.
[20] A. Pinelli, A. Vacca, A. Quarteroni, A spectral multidomain method for the numerical simulation of turbulent flows, J. Comput. Phys. 136 (1997) 546–558.
[21] C. Bernardi, Y. Maday, A.T. Patera, in: H. Brezis, J.L. Lions (Eds.), A New Non-conforming Approach to Domain Decomposition: The Mortar Element Method, vol. XI, Pitman, Boston, 1994, pp. 13–51.
[22] D.N. Arnold, F. Brezzi, B. Cockburn, L.D. Marini, Unified analysis of discontinuous Galerkin methods for elliptic problems, SIAM J. Numer. Anal. 39 (2002) 1749–1779.
[23] W. Couzy, M. Deville, A fast Schur complement method for the spectral element discretization of the incompressible Navier–Stokes equations, J. Comput. Phys. 116 (1995) 135–142.
[24] M.O. Deville, P.F. Fisher, E.H. Mund, High-order Methods for Incompressible Fluid Flow, Cambridge University Press, New York, 2002.

[25] L.F. Pavarino, O.B. Widlund, A polylogarithmic bound for an iterative substructuring method for spectral elements in three dimensions, SIAM J. Numer. Anal. 33 (1996) 1303–1335.
[26] M.A. Casarin, Quasi-optimal Schwarz methods for the conforming spectral element discretization, SIAM J. Numer. Anal. 34 (1997) 2482–2502.
[27] L.F. Pavarino, T. Warburton, Overlapping Schwarz methods for unstructured spectral elements, J. Comput. Phys. 160 (2000) 298–317.
[28] J. Van Kan, A second order accurate pressure correction scheme for viscous incompressible flow, SIAM J. Sci. Stat. Comput. 7 (1986) 870–891.
[29] J. Shen, On error estimates of the projection methods for the Navier–Stokes equations: second order schemes, Math. Comput. 65 (215) (1996) 1039–1065.
[30] C. Canuto, M.Y. Hussaini, A. Quarteroni, T.A. Zang, Spectral Methods In Fluid Dynamics, Springer, New York, 1988.
[31] G. Golub, C. Van Loan, Matrix Computations, The John Hopkins University Press, Baltimore, MD, 1989.
[32] C. Bernardi, Y. Maday, Approximations Spectrales de Problèmes aux Limites Elliptiques, Springer, Paris, 1992.
[33] T.F. Chan, D. Goovaerts, Schur complement domain decomposition algorithms for spectral methods, Appl. Numer. Math. 6 (1989) 53–64.
[34] T.F. Chan, T.P. Mathew, J.P. Shao, Efficient variants of the vertex space domain decomposition algorithm, SIAM J. Sci. Stat. Comput. 15 (6) (1994) 1349–1374.
[35] B.F. Smith, An optimal domain decomposition preconditioner for the finite element solution of linear elasticity problems, SIAM J. Sci. Stat. Comput. 13 (1) (1992) 364–378.
[36] J.H. Bramble, J.E. Pasciak, A.H. Schatz, The construction of preconditioners for elliptic problems by substructuring I, Math. Comput. 47 (175) (1986) 103–134.
[37] L.M. Carvalho, L. Giraud, P. Le Tallec, Algebraic two-level preconditioners for the Schur complement method, SIAM J. Sci. Comput. 22 (6) (2001) 1987–2005.
[38] M.A. Casarin, Diagonal edge preconditioners in p-version and spectral element methods, SIAM J. Sci. Comput. 18 (2) (1997) 610–620.
[39] A.T. Patera, Fast direct Poisson solvers for high-order finite element discretizations in rectangularly decomposable domains, J. Comput. Phys. 65 (1986) 474–480.
[40] M. Germano, U. Piomelli, P. Moin, W.H. Cabot, A dynamic subgrid scale eddy viscosity model, Phys. Fluids 3 (1991) 1760–1767.
[41] D.K. Lilly, A proposed modification of the Germano subgrid-scale closure method, Phys. Fluids 4 (3) (1992) 633–635.